

Estimating global and local scaling exponents in turbulent flows using discrete wavelet transformations

Gabriel Katul^{a)}

*School of the Environment, Duke University, Durham, North Carolina 27708-0328
and Center for Non-Linear and Complex Systems, Durham, North Carolina 27708*

Brani Vidakovic

Industrial and Systems Engineering, The Georgia Institute of Technology, Atlanta, Georgia 30032-0205

John Albertson

Department of Environmental Sciences, University of Virginia, Charlottesville, Virginia 22903

(Received 29 July 1999; accepted 21 September 2000)

High frequency longitudinal velocity (u) measurements were performed in the atmospheric surface layer to investigate the inertial subrange structure of turbulence. The u measurements, collected over a wide range of atmospheric stability conditions, were used to investigate local and global intermittency buildup in the inertial subrange. Global scaling exponents and other statistical properties were derived using nondecimated (NDWT) and critically sampled orthonormal (OWT) wavelet transformations. These statistical measures were contrasted to similar statistical measures derived by applying NDWT and OWT to an ensemble of fractional Brownian motion (fBm) time series with Hurst exponent of $1/3$. Such comparisons permit direct assessment as to whether discrepancies in observed intermittency corrections are artifacts of wavelet transformations or limitations in sample size. This study demonstrated that both NDWT and OWT were able to resolve intermittency-based departures from global power laws observed in higher-order structure functions of turbulence time series. Particularly, global power laws inferred from OWT and NDWT were consistent with new intermittency correction results derived from the dynamics of the fourth order structure functions. This study is the first to report on the ensemble behavior of such a power law for a wide range of surface boundary conditions (e.g., variable surface heating and friction velocity). The wavelet computed global intermittency departures from the classical Kolmogorov theory (or **K41**) were marginally smaller than those computed by the traditional structure function approach. In terms of local exponents, we found that the application of NDWT to fBm time series resulted in a wide empirical frequency distribution of local scaling exponents (α). The latter finding clearly demonstrates that previous and present α determined by wavelet analysis cannot be used as evidence for multifractality in turbulence. We also demonstrated that the classical local regression estimation of α is theoretically impaired by *heteroscedascity* when the local scale is finite. While the spread in α does not reflect any multifractal signatures, the modes of the local α frequency distribution support findings from global exponent analysis. We found that the modes of the local α distribution are well reproduced by global intermittency models for u and by **K41** for the fBm .
© 2001 American Institute of Physics. [DOI: 10.1063/1.1324706]

I. INTRODUCTION

Arguments that turbulence is not exactly self-similar, exhibits multifractal behavior, and possesses a distribution of local scaling exponents, were based on global statistical properties such as higher-order structure functions.^{1,2} Because of their ability to isolate dynamics in space and scale,^{3–6} several research efforts were dedicated to using continuous wavelet transformations (CWT) to estimate these local scaling exponents.^{2,7} In particular, Bacry *et al.*⁸ were the first to report local scaling exponent distributions of turbulent velocity calculated via CWT. Their results suggest that CWT can be used to estimate local scaling exponents

characterizing the multifractal behavior of velocity fluctuations without resorting to measures of turbulent kinetic energy dissipation. Additionally, their wind-tunnel measurements demonstrated that the mode of the local scaling exponent distribution is consistent with the Kolmogorov⁹ (hereafter referred to as **K41**) $1/3$ value. Also, the shape of the exponent-distribution appears to support the multifractal model of Parisi–Frisch.¹⁰ The main conclusions in Bacry *et al.*⁸ and others^{11,12} suggest the potential usefulness of CWT in understanding the local structure of turbulence. However, when CWT was applied to a fractional Brownian motion fBm time series exhibiting the same power spectrum as the turbulence time series, the local exponent probability density functions were similar. This consistency between fBm and turbulence local exponent distribution was also re-

^{a)} Author to whom correspondence should be addressed; electronic mail: gaby@duke.edu

ported in Vergassola *et al.*⁷ Some qualitative features, such as intensification of pitchfork patterns in the squared amplitudes of u vis-a-vis fBm were noted by Bacry *et al.*;⁸ however, the CWT could not quantitatively discern fundamental differences in local scaling exponent distributions between fBm and longitudinal velocity fluctuations (u). This led Vergassola *et al.*⁷ to argue that the similarity in local exponent histograms of u and fBm must be spurious and cautioned against the connection between a singularity spectrum of a multifractal process and the histogram of local exponents. The important role of local and global scaling exponents in developing a coherent theoretical framework for inertial subrange turbulence^{13–15} motivated us to further explore their estimation via wavelet transformations. Particularly, our objective is to evaluate whether an alternative wavelet-based approach, nondecimated wavelet transforms or NDWT, can delineate significant differences in scaling exponents between u and (fBm) time series. In fact, other researchers who utilized critically sampled orthogonal wavelet transformations (OWT) argued that the redundancy in CWT may well distort wavelet coefficients to the extent that dynamic properties of inertial subrange turbulence are masked rather than revealed.^{16–19} However, the traditional multiresolution format of OWT precludes detailed investigation of local scaling exponents at multiple time locations because of their limited resolution at coarse-grained scales. Because of these limitations in CWT and OWT, we propose an alternative wavelet-based approach to the determination of local and global scaling exponents, particularly, NDWT. The NDWT retains the desirable CWT redundancy in time but eliminates the redundancy in the scale domain. To date, NDWT have not been widely applied in turbulence research despite some of their potential advantages over CWT and OWT. Finally, while the usefulness of wavelet transformations to determine power laws has been realized in turbulence research,^{7,11,20–29} detailed power-law comparisons between these methods and structure function approaches have rarely been performed on the same data sets. Such a comparison, also presented here, is used to explore differences between NDWT- and OWT-derived global exponents and traditional structure function approaches.

II. THEORY

In this section, **K41** theory, properties of fBm , and the selection of the analyzing wavelet are reviewed. Appendix A provides an overview of NDWT and OWT.

A. K41 scaling

A property of the turbulent velocity differences ($u(x+r) - u(x)$) between two points separated by a distance r within the inertial subrange, for order $n > 1$, is given by

$$\langle [u(x+r) - u(x)]^n \rangle = C_n \langle \epsilon \rangle^{n/3} r^{n/3}, \tag{1}$$

where C_n are similarity constants (except for C_3) and $\langle \cdot \rangle$ denotes averaging. The turbulent kinetic energy dissipation rate ϵ is given by

$$\epsilon = \nu \langle s_{ij} s_{ij} \rangle,$$

where ν is the fluid kinematic viscosity, $s_{ij} = 1/2(\partial u_i / \partial x_j + \partial u_j / \partial x_i)$ is the strain rate tensor, u_1 (or u) is the turbulent longitudinal velocity component, u_2 (or v) is the turbulent lateral velocity component, and u_3 (or w) is the turbulent vertical velocity component, with $\langle u_i \rangle = 0$; x_i ($x_1 = x, x_2 = y, x_3 = z$) are the longitudinal, lateral, and vertical directions, respectively.

The above **K41** scaling laws hold for $\eta < r < L_u$, where $\eta = (\nu^3 / \langle \epsilon \rangle)^{1/4}$ is the Kolmogorov dissipation length scale and L_u is the integral length scale defined as

$$L_u = \frac{1}{\sigma_u^2} \int_0^\infty \langle u(x)u(x+r) \rangle dr,$$

for a stationary u .

B. Overview of fractional Brownian motion statistical properties

Energy cascades generated from solutions of the Navier–Stokes equations or simplifications to them (e.g., Shell models) are often contrasted with cascades generated by strictly self similar processes, such as fractional Brownian motion (fBm). Such comparisons highlight the role of multifractal properties of turbulence^{7,12,30} on many wavelet statistical measures. The fBm is a Gaussian, zero-mean, continuous, nonstationary process, indexed by the parameter H (Hurst exponent, $0 < H < 1$) such that

$$B_H(0) = 0, \quad \text{and} \quad B_H(t+r) - B_H(t) \sim \mathcal{N}(0, \sigma_H^2 |r|^{2H}),$$

where

$$\sigma_H^2 = \Gamma(1 - 2H) \frac{\cos \pi H}{\pi H},$$

and $\Gamma(x) = \int_0^\infty t^{x-1} e^{-t} dt$ is the Gamma function.^{21,31–33}

From its definition, the sample paths of fBm satisfy the scaling equation $B_H(at) = a^H B_H(t)$, and

$$\langle |B_H(t+r) - B_H(t)|^n \rangle = C_{fBm} \cdot |r|^{nH}, \tag{2}$$

where the C_{fBm} is

$$\sigma_H^2 \frac{2^{n/2} \Gamma\left(\frac{n+1}{2}\right)}{\Gamma\left(\frac{1}{2}\right)},$$

and where $\overset{d}{=}$ denotes *equal in distribution*.

The Fourier transformation of (2) is proportional to $1/|\omega|^{n(H+1/2)}$ with an average power spectrum proportional to $1/|\omega|^{2H+1}$. For $H = 1/3$ all **K41** global power laws are theoretically satisfied for any n . It is for this reason that an fBm time series with $H = 1/3$ is often referred to as a *Gaussian Kolmogorov signal*.⁷

C. Selection of wavelets

In wavelet transformations, the choice of the analyzing wavelet is not unique. Due to its wide usage in turbulence research,³⁴ and its suitability to this problem, we selected the

Haar wavelet, whose definition and properties are given in Appendix A. The Haar wavelet is antisymmetric so that statistical measures sensitive to vortex stretching can be well captured via its wavelet coefficients. In addition, the Haar wavelet is the most local of all wavelets in the time domain, making it suitable for resolving high intermittency levels in the signals. A discussion on the influence of the wavelet basis choice is also presented.

III. EXPERIMENT

Time series measurements were collected over a grass-covered forest clearing at Duke Forest near Durham, North Carolina. In this data set, 56 Hz velocity, and virtual potential temperature were collected on June 12–16 at 5.2 m above the grass surface using a GILL triaxial sonic anemometer. Sonic anemometers measure velocity by sensing the effect of wind on transit times of sound pulses traveling in opposite directions across a known instrument distance $d_{sl} = (0.149 \text{ m in this study})$. The measurements were subsequently divided into 19.5 min intervals to produce $N = 65\,536$ time measurement per run. Our choice of 19.5 min intervals is to ensure stationary conditions within a run. Here we focus on an ensemble of 103 runs collected over a wide range of atmospheric stability conditions ranging from near convective to stable atmospheric flows. In these runs, the friction velocity u_* varied from 0.04 to 0.47 m s^{-1} , and the sensible heat flux varied from -48 to 369 W m^{-2} . In short, the ensemble size exceeds 6.75×10^6 time measurement (but the analysis is conducted on individual runs prior to ensemble averaging). Since instrument averaging occurs for separation distances smaller than d_{sl} , we restrict the exponent and other statistical measure calculations to $r > d_{sl}$. Further details about the experimental setup, atmospheric conditions, inertial subrange identification, and instrumentation details can be found elsewhere.³⁵ In order to perform comparisons with a simulated fBm time series, each velocity run was normalized to zero-mean and unit variance.

IV. RESULTS

In this section, we consider global scaling exponents derived from structure functions, OWT, and NDWT and contrast our findings from these three global exponent estimator methods with established global intermittency models. We then utilize NDWT to estimate local scaling exponent distributions for both u and fBm and discuss whether NDWT can discern fundamental differences between cascades generated from Navier–Stokes turbulence and synthetic (or nonphysical) random processes.

A. Determination of global exponents

The global scaling exponents can be readily determined from the coefficients of NDWT or OWT using

$$\langle |\text{NDWT}_u(a, \cdot)|^n \rangle = C_\beta a^\beta,$$

where $\beta = -5/2 \cdot \zeta_n$ is the global exponent, C_β are constants related to the **K41** similarity constants (C_n) and $\langle \epsilon \rangle$, and $\langle \cdot \rangle$ is averaging across location for each scale a . Upon regress-

TABLE I. Selected models for ζ_n : **K41**, **K62** with intermittency exponent μ , monofractal β model with fractal dimension D , bifractal model, multifractal model with generalized dimension $D(h)$, She–Lévêque vortex filament model, and the Log-Stable model with parameter λ (related to helicity).

Model	ζ_n formulation	Parameters
K41 ^a	$\frac{n}{3}$	
K62 ^b	$\frac{n}{3} + \frac{\mu}{18}(3n - n^2)$	μ
Monofractal β ^c	$\frac{n}{3} + (3 - D)(1 - \frac{n}{3})$	D
Bifractal ^c	$\begin{cases} \frac{n}{3}, & n \leq 3 \\ \frac{n}{3}(3 - D)(1 - \frac{n}{3}), & n > 3 \end{cases}$	D
Multifractal ^c	$\inf_h [nh + 3 - D(h)]$	$D(h)$
She–Lévêque ^d	$\frac{n}{9} + 2 - 2(\frac{2}{3})^{n/3}$	
Log-Stable ^e	$\frac{n}{3} + 1 - \log_2[\lambda^{n/3} + (2 - \lambda)^{n/3}]$	λ

^aReference 9.
^bReference 47.
^cReference 2.
^dReference 48.
^eReference 38.

ing $\log\langle |\text{NDWT}_u(a, \cdot)|^n \rangle$ on $\log(a)$ for scales a within the inertial subrange, β can be estimated for all n .

To assess how well NDWT and OWT reproduce intermittency corrections, consider again the general n th order structure function given by

$$\langle |u(x+r) - u(x)|^n \rangle \propto r^{\zeta_n}, \tag{3}$$

where ζ_n is one of the models in Table I.

Figure 1 displays ζ_n computed from the structure function approach and from NDWT and OWT for both u and fBm . The fBm calculation, mainly used as a diagnostic for assessing limited sample size and run-to-run variability, is discussed next. Estimating the fBm ζ_n from the mean (or median) of the n th order structure function recovers **K41** well except when n is large (exceeds 6). In fact, the structure function estimated ζ_n for the fBm ensemble exhibits a spurious ζ_n that resembles a lognormal model with $\mu = 0.04$ (interestingly, consistent with the reported uncertainty for μ from many turbulence experiments³⁶). Additionally, the run-to-run global exponent variability in the structure function approach is much larger than say the OWT or NDWT methods. In short, the analysis on the fBm time series ensemble demonstrates that global exponents determined from OWT and NDWT are much more reliable and consistent from run-to-run when compared with their structure function counterpart. We emphasize here that the magnitude of the error bars is sensitive to the sample size, and perhaps, the turbulence conditions. However, the relative difference in error-bar magnitudes amongst methods indicates their robustness to determining scaling exponents.

For the u ensemble, the run-to-run variability in ζ_n is much larger (and skewed) for the structure function method when compared to OWT and NDWT. Some of this spurious behavior can be partially corrected via the so called *extended self-similarity* (ESS) approach,³⁷ in which the third order structure function is used as a normalizing measure.

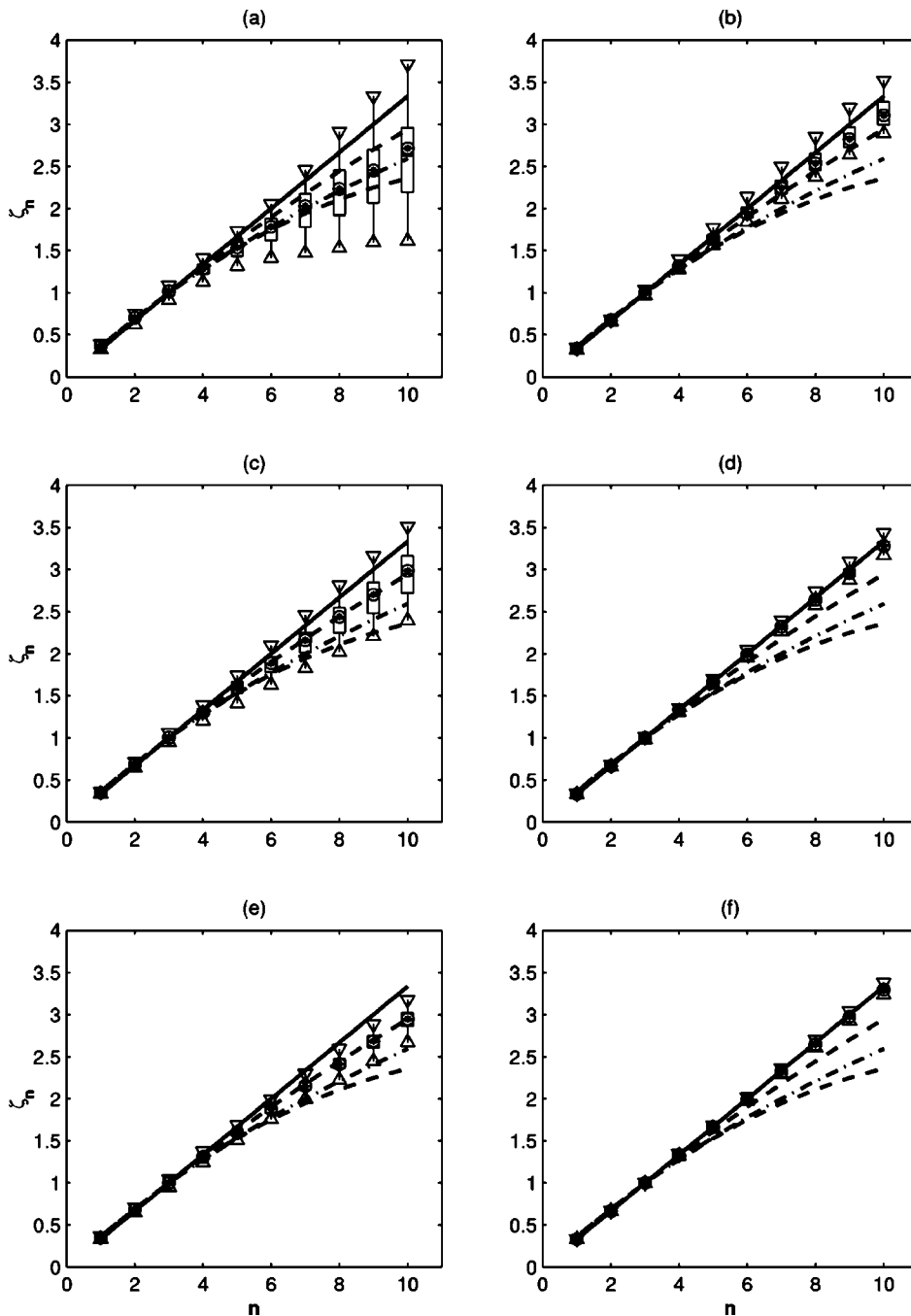


FIG. 1. Determination of ζ_n for $n = 1, 2, \dots, 10$ using structure functions (top panels), OWT (middle panels), and NDWT (lower panels). The left column is for the u ensemble and the right column is for the fBm ensemble. The vertical lines bound the minimum and maximum global exponents from all 103 runs, and the bars represent the 25% and 75% percentiles. The mean and median of the global exponent distributions are also shown (horizontal lines within the percentile bar). For reference, **K41**(solid), **K62** with $\mu = 0.1$ (Ref. 40) and $\mu = 0.25$ (dashed), and the She–Lévêque (dot-dashed) models are shown.

For clarity, a detailed comparison between the ζ_n for u as determined by the three methods is displayed in Fig. 2 along with reported measurements, simulations, and selected ζ_n models. It is clear that previous data sets estimate a ζ_n bounded by the She–Lévêque model and **K62** with $\mu = 0.25$ except for the Van Atta and Chen experiment. The latter experiment suffers from limited sample size,² especially for large n . Our ζ_n estimated from NDWT coefficients is much more consistent with **K62** with $\mu = 0.10$. Our large ζ_n relative to previous data sets cannot be attributed to a small sample size because such limitation usually leads to a reduction in ζ_n , not an increase. What is different about this experiment is that for each run the sampled u spectrum includes production and inertial scales, while other experiments spectrally sample u within the inertial and viscous

dissipation regimes. The direct numerical simulation reported in Sreenivasan and Dhruva¹⁴ is somewhat analogous to previous experiments because the resolved spectrum is predominantly inertial and dissipation. Similar statements can be made about the Shell Model³⁸ in its emphasis on cascades and dissipation (see also Ref. 39). To highlight why the inertial region, bounded by turbulent production end, offers different insights about intermittency behavior *vis-a-vis* inertial dissipation studies, we consider the recent theoretical work of Hayot and Jayaprakash.⁴⁰ It was noted by Hayot and Jayaprakash⁴⁰ that the refined similarity hypothesis of Kolmogorov, with

$$C_\epsilon(x, r) = \langle \epsilon(x+r)\epsilon(x) \rangle = \langle \epsilon \rangle^2 \left(\frac{r}{L_u} \right)^{-\mu},$$

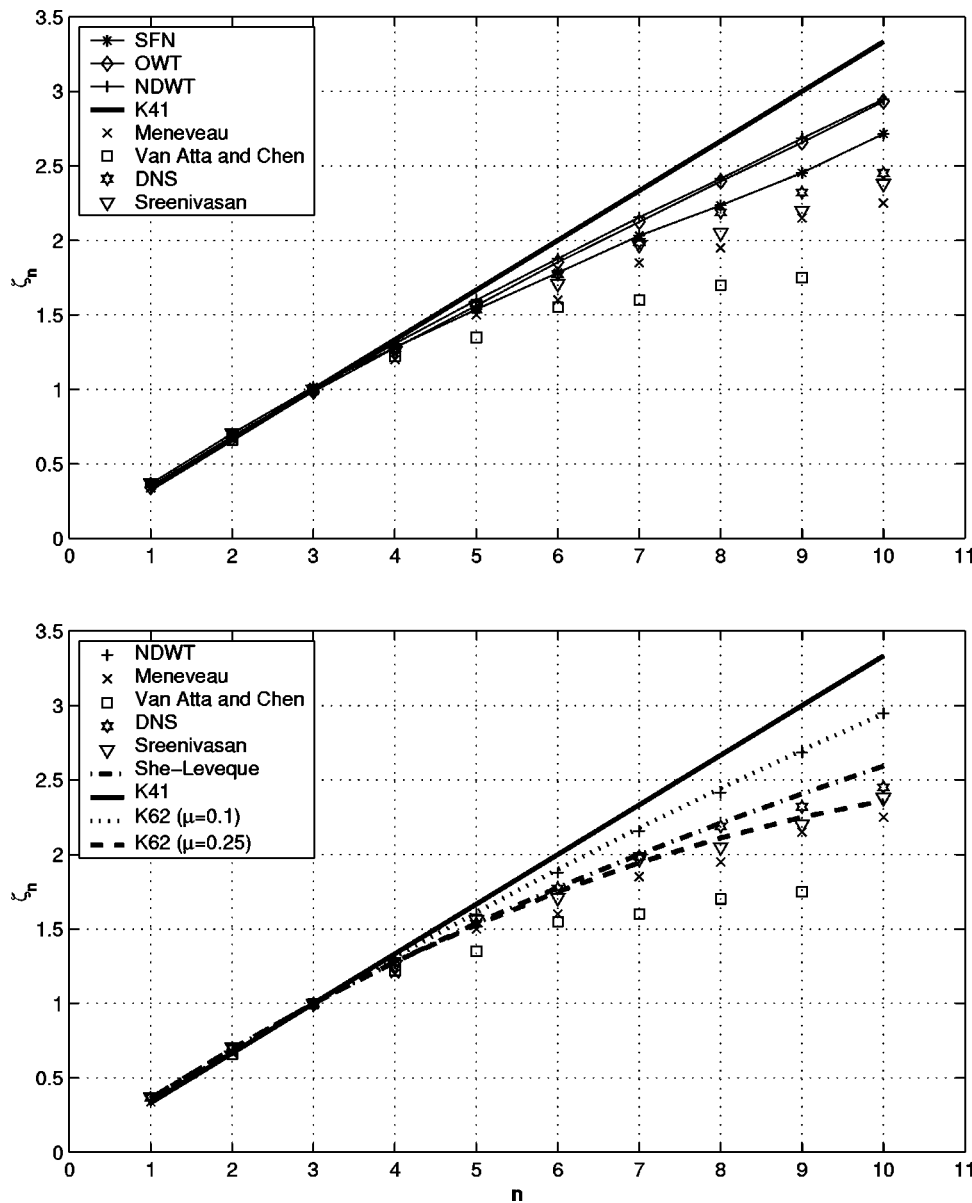


FIG. 2. (a) Determination of ζ_n for $n = 1, 2, \dots, 10$ for u using medians of the structure function (SFN) exponents, OWT, and NDWT. The data sets reported from other experiments include: boundary layer measurements from Meneveau *et al.* (Ref. 45), Van Atta and Chen (Ref. 49), and Benzi *et al.* (Ref. 37). Measurements from Anselmet *et al.* (Ref. 50) closely follow Meneveau *et al.* and are not shown. (b) Same as (a) but with the three intermittency models in Fig. 1 shown as lines. Simulational runs, e.g., direct numerical simulations of isotropic turbulence from Sreenivasan and Dhruva (Ref. 14), and GOY Shell Model (Ref. 38) are also shown. For reference, we repeat **K62** with $\mu = 0.1$ (Ref. 40) and $\mu = 0.25$ (Ref. 36), the She–Léveque model, and the Log-Stable model with $\lambda = 1.33$ estimated by us for this data set. For clarity, the NDWT-calculated ζ_n is also repeated.

leads to two intermittency exponents: $\mu_1 = 2 - \zeta_6$ and $\mu_2 \approx 2\zeta_2 - \zeta_4$. These two μ formulations were derived, in the equal time limit, from the Navier–Stokes equations for locally homogeneous and isotropic turbulence and from the one-dimensional stochastic Burgers equation.⁴⁰ The μ_2 term arises because a Galilean noninvariant term, known to contain sweeping effects, is significant in the formal equation for $C_\epsilon(x, r, t)$. In fact, these two μ models have already been recognized in earlier intermittency treatments.⁴¹ Based on published experimental values for ζ_2 , ζ_4 , and ζ_6 , Hayot and Jayaprakash estimate $\mu_1 = 0.25$ and $\mu_2 = 0.1$. As evidenced from Fig. 2, the NDWT estimated ζ_n is much more consistent with $\mu_2 = 0.1$ than $\mu_1 = 0.25$. Hayot and Jayaprakash demonstrated that when $r \ll L_u$, μ_1 predominantly influences ζ_n . While clear spectral signatures of the inertial subrange are evident in our experiments, the onset of the inertial scale (even for large n) are one order of magnitude smaller than L_u . It is likely that sweeping effects and other arguments leading to μ_2 are more appropriate than μ_1 when the u time

series runs are spectrally sampled in the production and inertial scales⁴⁰ (*vis-a-vis* inertial and viscous dissipation scales). The relative importance of sweeping effects on the inertial subrange structure for a similar data set, collected by us at this site, is reported elsewhere.⁴² In the latter experiment and others (e.g., Ref. 43), it was demonstrated that sweeping effects on higher-order statistics diminish with decreasing r within the inertial subrange. The fact that sweeping effects are significant for large r but negligible for smaller r within the inertial subrange serves to explain the contrasting $\mu_2 = 0.1$ in this study and $\mu_1 = 0.25$ for the inertial-viscous data sets. Other atmospheric surface layer studies hinted at potential differences in μ estimates depending on whether the production-inertial region or the inertial-dissipation region are used in the μ calculations. For example, Chambers and Antonia⁴⁴ found that $\mu = 0.15$ and $\mu = 0.25$ best fit their inertial subrange measurements interfacing the production and dissipation ends, respectively. The latter μ is identical to the *accepted* value from many other

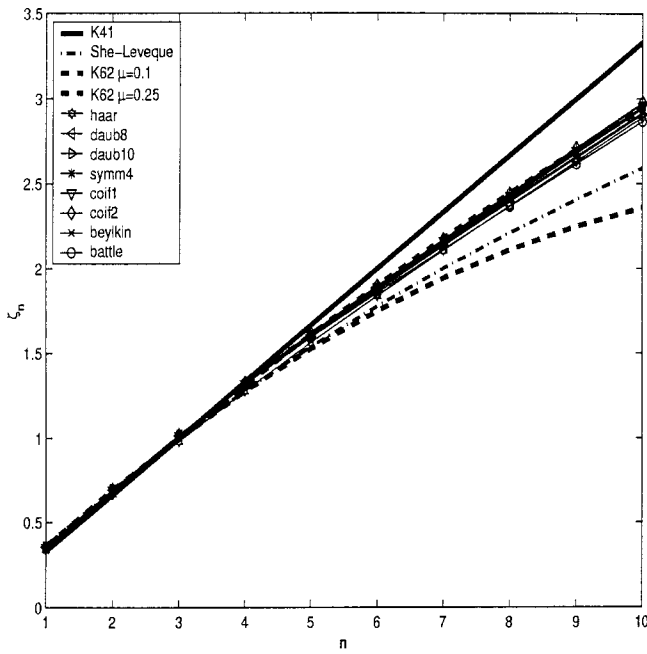


FIG. 3. Determination of ζ_n for $n=1,2,\dots,10$ for all 103 u runs using a library of OWT. For reference, the three global intermittency models for ζ_n in Fig. 1 are repeated.

laboratory studies.³⁶ It is difficult to generalize the experimental findings of Chambers and Antonia given their limited number of runs (4 runs compared to 103 in this study) and their use of structure function calculations. However, the trends in their μ are consistent with the low μ from our experiment and the larger μ from previous experiments.

We restate here that it is not our intent to investigate the accuracy of **K62** or other intermittency models of ζ_n but rather to highlight potential differences between previous experimental findings and the present experiment in light of the Hayot–Jayaprakash study. Consequences for other ζ_n models, such as the Log-Stable model, are equally applicable. For example, the Log-Stable model reproduces well the NDWT estimated ζ_n for a $\lambda=1.33$ (at least for $n\leq 10$). For reference, the value of λ , a parameter related to helicity, must be 1.0 to recover **K41**. For matching the data set of Meneveau *et al.*⁴⁵ by the Log-Stable model, $\lambda=1.42$, somewhat larger than our 1.33. These λ differences may again be attributed to the relative importance of sweeping effects on inertial subrange statistics.

Finally, in order to verify that our results are not sensitive to the choice of the wavelet basis, we repeated the entire analysis for the 103 runs using a library of compactly supported orthonormal wavelets. This analysis demonstrated that the effect of the basis function is minor as evidenced in Fig. 3.

B. Determination of local exponents

A motivation for using CWT or NDWT is in their ability to estimate local scaling exponents. The local scaling exponents can be estimated from NDWT using local regularity results.⁶ At locations where u has a Lipschitz regularity³ α , the localized energy $(CWT_u(a,b))^2$ behaves as $a^{2\alpha+1}$, for

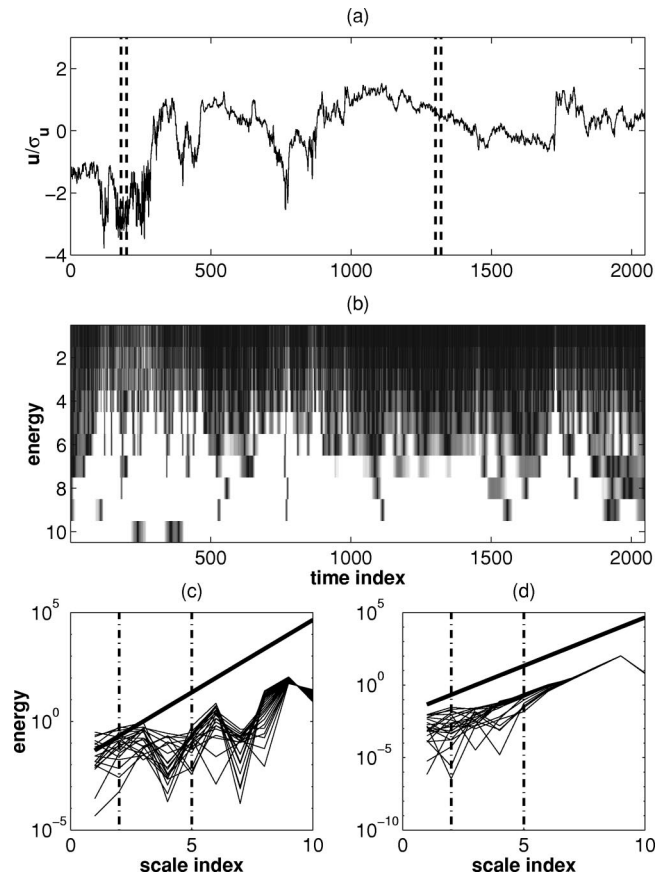


FIG. 4. (a) A sample of measured time series (36.57 s) of normalized u indexed from 1 to 2048. The vertical dashed lines (indices 180–200 and 1300–1320) indicate regions for which the local spectra are displayed. (b) The NDWT squared amplitudes in the wavelet halfplane of the time series in (a). Light colors represent large squared amplitudes (or large energy content). (c) The ensemble of local energy spectra for indices 180 to 200 of the time series in (a). (d) Same as (c) but for indices 1300 to 1320. In panels (c) and (d), the solid line is **K41** power law for $n=2$.

scale a within the inertial subrange. Hence, α at position b may be estimated from the local energy spectrum as discussed in Ref. 28. To illustrate the traditional estimation of α , consider 36.57 s (indexed from 1 to 2048) of a normalized u time series measurement (normalized to zero mean and unit variance) in concert with their $(NDWT_u(a,b))^2$. We estimated α in the vicinity of large and small u time gradients (Fig. 4) by regressing $\log_2([NDWT_u(a,b)]^2)$ on $\log_2 a$. Figure 4 suggests that negative exponents can occur in regions experiencing rapid transients in u , consistent with Bacry *et al.* The quiescent periods approximately follow **K41** as evidenced by the local wavelet spectra shown in panel (d). Hence, it may be expected that a large α coincides with large excursions in u , but most of the α 's to be concentrated in the neighborhood of the global ζ_n . This local regression estimation method suffers from several theoretical limitations for finite a and we assess them later in this section. Nonetheless, using such a local regression method, we estimated α for the entire u and fBm 103 runs (each of sample size $N=65\,536$) and present the ensemble frequency distributions of the 6,750,208 α in Fig. 5 for u and fBm and for $n=1$ in panel (a) along with Bacry *et al.*'s reported frequency distribution (digitized by us), $n=2$ in panel (b) and

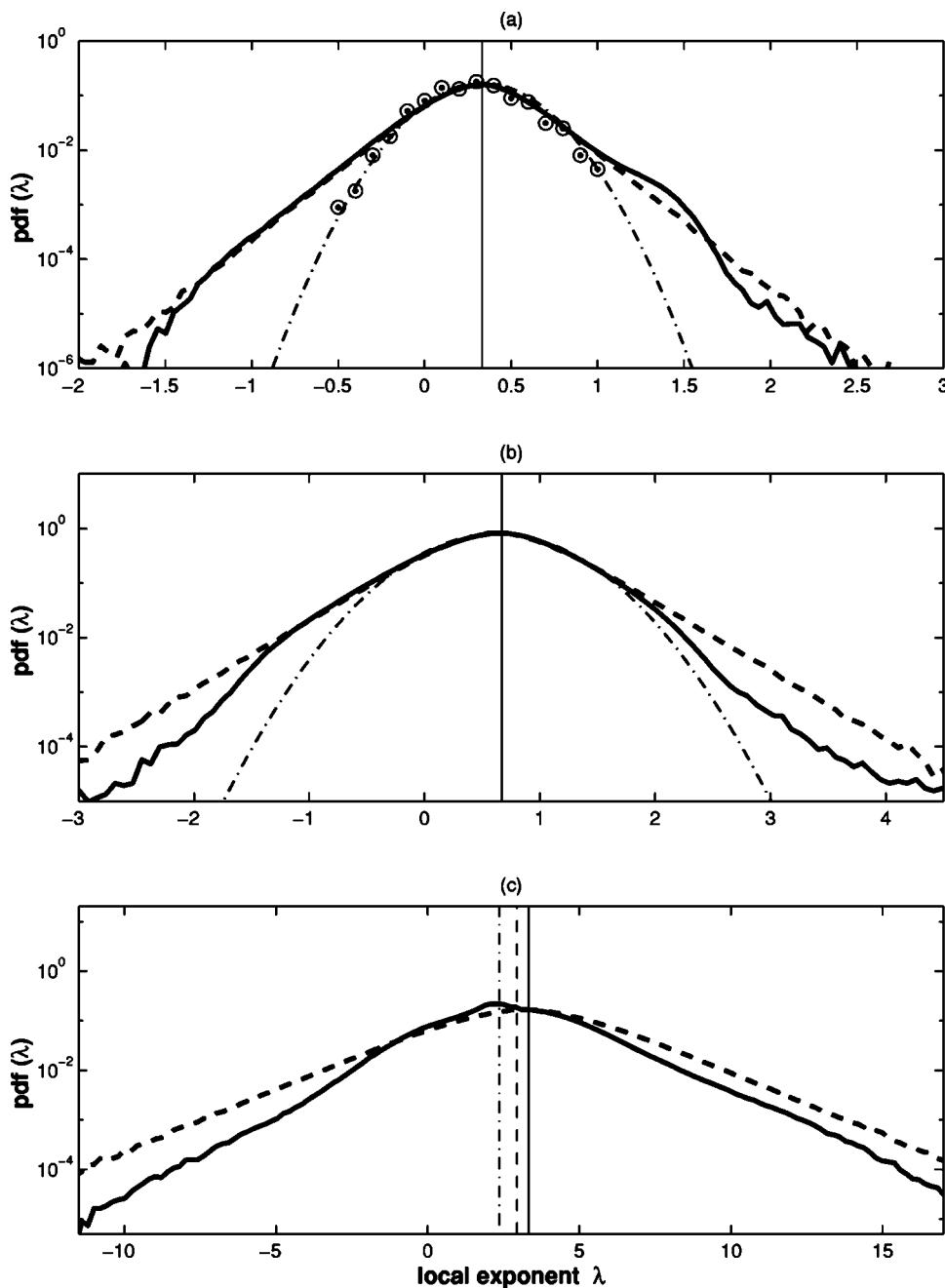


FIG. 5. The frequency distribution (or pdf) of the local exponent α for $n = 1$ (panel a), $n = 2$ (panel b), and $n = 10$ (panel c). In all three panels, the solid line and dashed lines are for u and fBm , respectively. For reference, Bacry *et al.* only reported frequency distribution for $n = 1$, are shown. To illustrate the decay at the tails, a Gaussian pdf (dot-dashed line) is also shown.

$n = 10$ in panel (c). Bacry *et al.*'s local exponent is displayed to simply illustrate the limited frequency distribution tails considered in their study relative to our surface layer measurements. It appears that both u and fBm time series exhibit a wide distribution of local exponents. Hence, such frequency exponent analysis can not be used as proof of multifractality as was done by Bacry *et al.* since the fBm is theoretically not multifractal. Vergassola *et al.*⁷ suggest that the large and spurious α distribution for both fBm and u may be due to the noise created upon regressing $\log_2([CWT_u(a,b)]^2)$ on $\log_2 a$.

To further investigate this point, we repeated the α frequency distribution analysis using two independent regression-noise suppression methods: selecting only α values for which the regression correlation coefficient exceeded

0.98, and selecting α values for which a dimensionless measure of linearity exceed 0.98. The linearity measure is defined as the inverse ratio of the sum of all distances connecting a sequence of coordinate points to the distance between the two farthest points (farthest on the abscissa or $\log(a)$ axis). We found that the latter measure does not exclude near-zero α values as the correlation coefficient measure inherently does (near-zero α are associated with small correlation coefficients). The spread reduction in α distribution was minimally affected upon conditioning on either of these two methods, particularly for the fBm runs. That is, such a spread in α cannot be an artifact of the weak linearity between $\log|NDWT(a,b)|^n$ and $\log a$.

In Appendix B, we demonstrate that regressing $\log|NDWT(a,b)|^n$ on $\log a$ leads to a theoretical error term

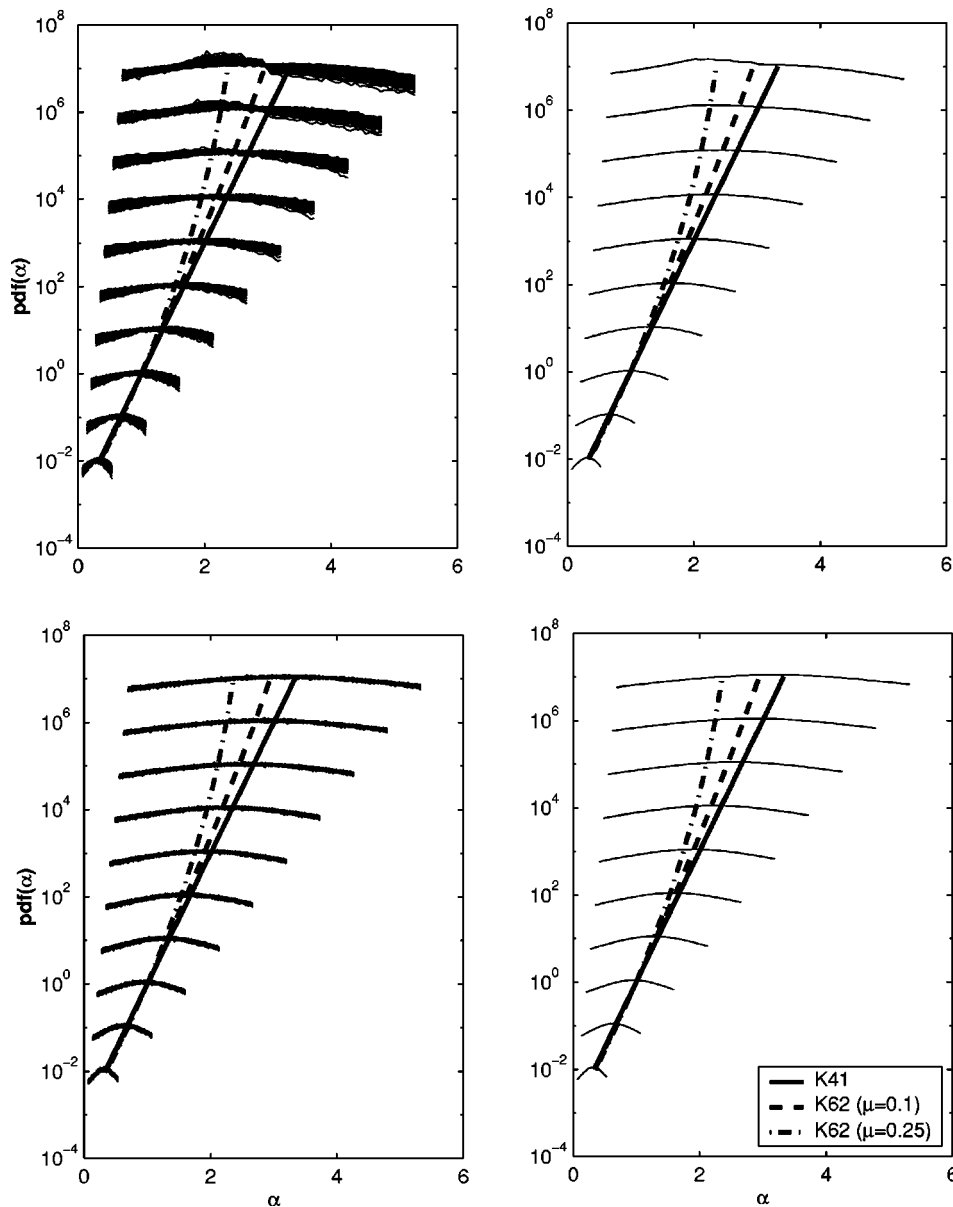


FIG. 6. The NDWT local exponent (α) probability density functions. Top panels are for u and bottom panels are for the fBm ensemble. The left panels show the $pdf(\alpha)$ for $n=1,2,\dots,10$, with $n=1$ being the smallest and the remaining $pdfs$ are shifted by one decade sequentially. The right panels are derived from the left panels by averaging all 103 $pdfs$ at each n and are displayed for clarity. The solid line represents **K41**, which describes well the fBm pdf modes, and the dashed and dot-dashed lines represent the two **K62** ζ_n models.

that is scale dependent. The conclusion from Appendix B is that when the scale a increases, local regularity results become inaccurate and the magnitude of the error term increases with scale. In short, determining α from such regression analysis is theoretically impaired by heteroscedasticity of an error term.

To assess the sensitivity of all the α calculations to the range of scales defining the inertial subrange, several inertial scale subranges were considered. We found that the least squares estimator of the slope remains stable even if the inertial subrange scale limits were perturbed by 50%.

Here, we propose an alternative application of the α frequency distribution that is useful in estimating ζ_n . This alternative application stems from the fact that even when the noise is heteroscedastic, its ensemble average is zero. In Fig. 6, the modes of the local α frequency distribution for $n = 1, 2, \dots, 10$ are well reproduced by **K62** with $\mu=0.1$ for u and by **K41** for the fBm consistent with the global exponents. That is, the most probable exponent (for a wide range

of runs) calculated by NDWT is nearly identical to the global exponent. In short, local exponent analysis may be used to support global exponent calculations. However, any inference about the distributions of α may be compromised by the heteroscedastic noise.

V. CONCLUSION

Using an ensemble of longitudinal velocity measurements, collected over a wide range of friction velocity and surface heating conditions, we demonstrated the following:

- (i) Orthonormal and nondecimated wavelet transformation provide more robust global exponent estimators when compared to their structure function counterpart, particularly for higher-order n . When contrasting discrete wavelet transforms with structure function approaches, we note that the wavelet transformation has an adaptive scale smoothing kernel (as evidenced from the Fourier transformations of decomposing

wavelets). This smoothing is not generally conducted when structure functions are employed. Hence, it is not surprising that global slopes determined from wavelets are less influenced by local scale scatter. To explain the difference between the two wavelet methods, recall that NDWT does not decimate, thereby retaining at each scale a number of coefficients identical to the length of the input time series. Hence, averaging across coefficients at each scale is more stable when NDWT is contrasted with critically sampled OWT. In short, the combination of smoothing in the scale domain and redundancy in the time domain makes NDWT the most robust global slope estimator when contrasted to structure functions and OWT.

- (ii) The application of orthonormal and nondecimated wavelet transformations to the ensemble atmospheric velocity measurements revealed new insights about the global exponent ζ_n in the inertial subrange as bounded by the turbulent production. For example, a lognormal model with intermittency parameter $\mu = 0.1$ better matches the measurements when compared to the accepted $\mu = 0.25$ (derived from inertial-dissipation measurements). The $\mu = 0.1$ is consistent with the two intermittency exponent argument in Hayot and Jayaprakash in which the smaller μ arises when sweeping effects are significant.
- (iii) The use of nondecimated wavelet transforms to infer local exponents revealed that both fBm and turbulence have a wide distribution of such local scaling exponents. We have shown that such a spread is a consequence of heteroscedascity in the noise term and results in a poor connection between local exponents derived from wavelet analysis for finite scales and the singularity spectrum of a multifractal process. Hence, the presence of a local scaling exponent as derived from such analysis (or a variant as in Bacry *et al.*) does not prove or disprove the multifractal characteristics of turbulence. Nonetheless, the measures of location of such distributions (e.g., mean, median, or mode) are consistent with their inferred global exponent values (i.e., ζ_n is $n/3$ for fBm and lognormal with $\mu = 0.1$ for turbulence). This consistency can be attributed to the theoretical zero-mean value of the heteroscedastic noise.

ACKNOWLEDGMENTS

This project was funded by the National Science Foundation (Grants Nos. DMS-9626159, EAR-99-03471, and BIR-95-12333).

We thank D. Donoho for providing us with a beta version of WAVELAB 0.8 which was used in all the wavelet calculations. The MATLAB *m*-files and *u* data sets are available upon request from the authors.

APPENDIX A: AN OVERVIEW OF NONDECIMATED AND CRITICALLY SAMPLED DISCRETE WAVELET TRANSFORMATIONS

In this Appendix, definitions and important properties of nondecimated wavelet transformations (NDWT) and their critically sampled counterparts (OWT) are presented. For quadrature mirror filters h and g , we define recursive up-sampled filters $h^{[r]}$ and $g^{[r]}$,

$$h^{[0]} = h, \quad g^{[0]} = g,$$

$$h^{[r]} = [\uparrow/2]h^{[r-1]}, \quad g^{[r]} = [\uparrow/2]g^{[r-1]}.$$

In practice, the dilated filter $h^{[r]}$ is obtained by inserting zeros between the taps in $h^{[r-1]}$. Let $\mathbf{H}^{[r]}$ and $\mathbf{G}^{[r]}$ be convolution operators with filters $h^{[r]}$ and $g^{[r]}$, respectively. A nondecimated wavelet transformation is defined as a sequential application of operators (convolutions) $\mathbf{H}^{[j]}$ and $\mathbf{G}^{[j]}$ on a given time series.

Definition. Let $a^{(J)} = c^{(J)}$ and

$$a^{(j-1)} = \mathbf{H}^{[J-j]}a^{(j)}, \quad b^{(j-1)} = \mathbf{G}^{[J-j]}a^{(j)}.$$

The nondecimated wavelet transformation of $c^{(J)}$ is $b^{(J-1)}, b^{(J-2)}, \dots, b^{(J-j)}, a^{(J-j)}$, for some $j \in \{1, 2, \dots, J\}$ the depth of the transformation.

If the length of an input vector $c^{(J)}$ is 2^J , then for any $0 \leq m < J$, $a^{(m)}$ and $b^{(m)}$ are of the same length. Let $\phi_j(x) = \phi_{j,0}(x)$ and $\psi_j(x) = \psi_{j,0}(s)$. If the measurement sequence $c^{(J)}$ is associated with the function $f(x) = \sum_k c_k^{(J)} \phi_j(x - 2^{-j}k)$ then the k th coordinate of $b^{(j)}$ is equal to

$$b_{jk} = \int \psi_j(x - 2^{-j}k) f(x) dx.$$

Thus, the coefficient b_{jk} provides information at scale 2^{J-j} and location k . One can think of a nondecimated wavelet transformation $\langle f(x), (1/\sqrt{a}) \psi((x-b)/a) \rangle$ for $a = 2^{-j}$, and $b = k$. The OWT is defined by the critical sampling given by

$$a = 2^{-j}, \quad b = k2^{-j}, \quad j, k \in \mathbb{Z},$$

and will produce a minimal basis. Any coarser sampling will not provide a unique inverse transformation. That is, the original function will not be uniquely recoverable. For appropriate conditions applied to the wavelet function ψ , such sampling produces an orthonormal basis $\{\psi_{jk}(x) = 2^{j/2} \psi(2^j x - k), j, k \in \mathbb{Z}\}$. The coefficients of a function in the orthonormal wavelet basis represent orthonormal wavelet transformation, OWT. One such basis function, used in this study, is generated by shifts and scales of a function

$$\psi(x) = \mathbf{1}(0 \leq x \leq 1/2) - \mathbf{1}(1/2 \leq x \leq 1).$$

This function, known as the Haar wavelet, is used frequently in turbulence research.³⁴ Wavelet packets have also been proposed as an alternative source of basis functions in turbulence research.²⁷ When compared with the Haar wavelet in the context of energy packing, only minor improvements were reported.³⁴ Hence, for the purposes of this study, only Haar's OWT is considered.

APPENDIX B: ERRORS IN LOCAL SLOPE ESTIMATION

In this technical Appendix we demonstrate that the local slope estimation errors are scale dependent quantities and amplify as the scale increases.

Let $\text{CWT}_Y(a,b) = \int Y(t)\psi_{a,b}(t)dt$ be the continuous wavelet transformation of the measured time series $Y(t)$, where $\psi_{a,b}(t) = 1/\sqrt{a}\psi((t-b)/a)$, and ψ an admissible decomposing wavelet. For $a \rightarrow 0$, local regularity result implies that

$$\langle |\text{CWT}_Y(a,b)|^n \rangle \sim C_1 \cdot a^\beta, \quad (\text{B1})$$

where $\langle \cdot \rangle$ is ensemble averaging.

At a given time instant (or translation) b , $y(a) = \log |\text{CWT}_Y(a,b)|^n$ can be observed.

Let

$$C_2 = \left\langle \log \left\{ \frac{|\text{CWT}_Y(a,b)|^n}{\langle |\text{CWT}_Y(a,b)|^n \rangle} \right\} \right\rangle$$

and

$$\varepsilon_n(a) = \log \frac{|\text{CWT}_Y(a,b)|^n}{\langle |\text{CWT}_Y(a,b)|^n \rangle} - C_2.$$

Then, when $a \rightarrow 0$, $y(a)$ can be expressed as

$$y(a) = C_2 + \log \langle |\text{CWT}_Y(a,b)|^n \rangle + \varepsilon_n(a).$$

Using (B1), $y(a)$ behaves as

$$y(a) \sim C + \beta \cdot \log a + \varepsilon_n(a), \quad (\text{B2})$$

for $C = \log C_1 + C_2$.

Since $\varepsilon_n(a)$ is not 0 for finite a , it is impossible to determine β exactly by locally regressing $y(a)$ on $\log a$ (even if the coefficient of correlation between $y(a)$ and $\log a$ is ± 1). When a increases the approximation (B1) becomes inaccurate, and the magnitude of $\varepsilon_n(a)$ increases as well. In short, the determining of β from (B2) is impaired by heteroscedascity of the error term $\varepsilon_n(a)$ (Ref. 46, p. 423). Similar arguments apply for $|\text{NDWT}_Y(a,b)|^n$.

¹K. R. Sreenivasan, R. A. Antonia, and D. Britz, *J. Fluid Mech.* **94**, 745 (1979).

²U. Frisch, *Turbulence* (Cambridge University Press, New York, 1995), p. 296.

³M. Holschneider, *Wavelets: An Analysis Tool* (Oxford Science, Oxford, 1995), p. 423.

⁴*Wavelets and Applications, Research Notes in Applied Mathematics*, No. 26, edited by Y. Meyer (Springer-Verlag, New York, 1991).

⁵Y. Meyer, *Wavelets and Operators, Cambridge Studies in Advanced Mathematics* (Cambridge University Press, New York, 1992), Vol. 37.

⁶S. G. Mallat, *A Wavelet Tour of Signal Processing* (Academic, San Diego, 1998).

⁷M. Vergassola, R. Benzi, L. Biferale, and D. Pisarenko, *J. Phys. A* **26**, 6093 (1993).

⁸E. Bacry, A. Arneodo, U. Frisch *et al.*, in *Turbulence and Coherent Structures*, edited by O. Metais and M. Lesieur (Kluwer Academic, Norwell, MA, 1991), p. 450.

⁹A. N. Kolmogorov, *Dokl. Akad. Nauk SSSR* **4**, 299 (1941).

¹⁰G. Parisi and U. Frisch, in *Turbulence and Predictability in Geophysical Fluid Dynamics*, edited by M. Ghil, R. Benzi, and G. Parisi (North-Holland, Amsterdam, 1985).

¹¹F. Argoul, A. Arneodo, G. Grasseau *et al.*, *Nature (London)* **338**, 51 (1989).

¹²R. Everson, L. Sirovich, and K. Sreenivasan, *Phys. Lett. A* **145**, 314 (1990).

¹³Z.-S. She, *Prog. Theor. Phys.* **130**, 87 (1998).

¹⁴K. R. Sreenivasan and B. Dhruva, *Prog. Theor. Phys.* **130**, 103 (1998).

¹⁵K. R. Sreenivasan and R. A. Antonia, *Annu. Rev. Fluid Mech.* **29**, 435 (1997).

¹⁶M. Yamada and K. Ohkitani, *Prog. Theor. Phys.: Prog. Lett.* **86**, 819 (1990).

¹⁷M. Yamada and K. Ohkitani, *Fluid Dyn. Res.* **8**, 101 (1991).

¹⁸M. Yamada and K. Ohkitani, *Prog. Theor. Phys.* **86**, 799 (1991).

¹⁹G. G. Katul, J. D. Albertson, C. C. Chu, and M. B. Parlange, in *Wavelets in Geophysics*, edited by E. Foufoula (Academic, San Diego, 1994), pp. 81–105.

²⁰L. Hudgins, C. A. Friehe, and M. E. Mayer, *Phys. Rev. Lett.* **71**, 3279 (1993).

²¹A. Benassi, in *Lecture Notes in Statistics*, edited by A. Antoniadis and G. Oppenheim (Springer-Verlag, New York, 1995), Vol. 103.

²²R. Benzi and M. Vergassola, *Fluid Dyn. Res.* **8**, 117 (1991).

²³M. Farge, *Annu. Rev. Fluid Mech.* **24**, 395 (1992).

²⁴C. Meneveau, *J. Fluid Mech.* **232**, 469 (1991).

²⁵C. Meneveau, *Phys. Rev. Lett.* **11**, 1450 (1991).

²⁶G. G. Katul and M. B. Parlange, *J. Atmos. Sci.* **51**, 2181 (1994).

²⁷M. Farge, E. Goirand, Y. Meyer *et al.*, *Fluid Dyn. Res.* **10**, 229 (1992).

²⁸J. Liandrat and F. Moret-Bailly, *Eur. J. Mech. B/Fluids* **9**, 1 (1990).

²⁹M. Vergassola and U. Frisch, *Physica D* **54**, 58 (1991).

³⁰L. Biferale, *Phys. Fluids A* **5**, 428 (1993).

³¹P. Flandrin, *IEEE Trans. Inf. Theory* **35**, 197 (1989).

³²P. Flandrin, in *Wavelets and Their Applications*, edited by J. S. Byrnes, J. L. Byrnes, K. A. Hargreaves, and K. Berry, NATO ASI Series (Kluwer, Dordrecht, 1992), Vol. 442, pp. 121–142.

³³P. Flandrin, *IEEE Trans. Inf. Theory* **38**, 910 (1992).

³⁴G. G. Katul and B. Vidakovic, *J. Atmos. Sci.* **55**, 377 (1998).

³⁵G. Katul, C. Hsieh, and J. Sigmon, *Boundary-Layer Meteorol.* **82**, 49 (1997).

³⁶K. Sreenivasan and P. Kailasnath, *Phys. Fluids A* **5**, 512 (1993).

³⁷R. Benzi, S. Ciliberto, R. Tripicciono *et al.*, *Phys. Rev. E* **48**, R29 (1993).

³⁸E. Leveque and Z. She, *Phys. Rev. E* **55**, 2789 (1997).

³⁹M. Iima and S. Toh, *J. Phys. Soc. Jpn.* **67**, 4068 (1998).

⁴⁰F. Hayot and C. Jayaprakash, *Phys. Fluids* **12**, 327 (2000).

⁴¹M. Nelkin and T. Bell, *Phys. Rev. A* **17**, 363 (1978).

⁴²G. Katul, M. Parlange, J. Albertson, and C.-R. Chu, *Fluid Dyn. Res.* **16**, 275 (1995).

⁴³A. Praskovskiy, E. Gledzerm, M. Karyakin, and Y. Zhou, *J. Fluid Mech.* **248**, 493 (1993).

⁴⁴A. Chambers and R. Antonia, *Boundary-Layer Meteorol.* **28**, 343 (1984).

⁴⁵C. Memeveau, K. R. Sreenivasan, P. Kailasnath, and M.-S. Fan, *Phys. Rev. A* **41**, 894 (1990).

⁴⁶J. Netter, W. Wasserman, and M. Kutner, *Applied Linear Regression Models* (Irwin, Homewood, IL, 1989).

⁴⁷A. N. Kolmogorov, *J. Fluid Mech.* **13**, 82 (1962).

⁴⁸Z. She and E. Leveque, *Phys. Rev. Lett.* **72**, 336 (1994).

⁴⁹C. W. V. Atta and W. Y. Chen, *J. Fluid Mech.* **44**, 145 (1970).

⁵⁰F. Anselmet, Y. Gagne, E. J. Hopfinger, and R. A. Antonia, *J. Fluid Mech.* **140**, 63 (1984).